Nonlinear elastic response of strong solids: First-principles calculations of the third-order elastic constants of diamond

A. Hmiel, J. M. Winey, and Y. M. Gupta
Institute for Shock Physics and Department of Physics, Washington State University, Pullman, Washington 99164, USA

M. P. Desjarlais
Sandia National Laboratories, Albuquerque, New Mexico 87185, USA

(Received 18 January 2016; revised manuscript received 15 March 2016; published 23 May 2016)

Accurate theoretical calculations of the nonlinear elastic response of strong solids (e.g., diamond) constitute a fundamental and important scientific need for understanding the response of such materials and for exploring the potential synthesis and design of novel solids. However, without corresponding experimental data, it is difficult to select between predictions from different theoretical methods. Recently the complete set of third-order elastic constants (TOECs) for diamond was determined experimentally, and the validity of various theoretical approaches to calculate the same may now be assessed. We report on the use of density functional theory (DFT) methods to calculate the six third-order elastic constants of diamond. Two different approaches based on homogeneous deformations were used: (1) an energy-strain fitting approach using a prescribed set of deformations, and (2) a longitudinal stress-strain fitting approach using uniaxial compressive strains along the [100], [110], and [111] directions, together with calculated pressure derivatives of the second-order elastic constants. The latter approach provides a direct comparison to the experimental results. The TOECs calculated using the energy-strain approach differ significantly from the measured TOECs. In contrast, calculations using the longitudinal stress-uniaxial strain approach show good agreement with the measured TOECs and match the experimental values significantly better than the TOECs reported in previous theoretical studies. Our results on diamond have demonstrated that, with proper analysis procedures, first-principles calculations can indeed be used to accurately calculate the TOECs of strong solids.

DOI: 10.1103/PhysRevB.93.174113

I. INTRODUCTION

The synthesis, investigation, and computational design of strong solids (also known as ultrahard materials) are of significant ongoing scientific interest to fields like solid state physics, geophysics, nanoscience, and high-pressure physics [1–6] and have applications in wide-ranging areas like abrasives, biomedical sciences, superconductive materials, and defense technologies [7–9]. A detailed understanding of the mechanical response of these materials is important because many potential applications involve large and/or highly nonuniform applied stresses. The elastic constants are fundamental to understanding the mechanical response: the second-order elastic constants (SOECs) characterize the linear elastic response, and the third-order elastic constants (TOECs) characterize the lowest-order nonlinear elastic response.

Determination of the TOECs of crystals has a long history in solid state physics because they reflect the lowest-order nonlinear (anharmonic) contributions to the lattice potential [10]. Therefore, the TOECs are important for understanding physical phenomena related to lattice anharmonicity such as phonon-phonon interactions, thermal expansion, and stress- and temperature-dependent elastic response [11,12]. For ultrahard materials, such as diamond, experiments to investigate their nonlinear elastic properties are particularly challenging. Therefore, theoretical determination of the TOECs for such materials is of significant importance.

Although theoretical calculations of the diamond TOECs have been reported previously [13–17], two shortcomings in these studies are noteworthy: significant differences existed between the reported values, and experimentally determined values of the full set of diamond TOECs were not available. Hence, it was difficult to evaluate the validity of the various theoretical approaches. In 2011, Lang and Gupta [18] reported an experimental determination of the full set of TOECs for diamond by combining their shock compression data [18,19] along three different crystal orientations with previously reported pressure derivatives of the SOECs [20]. Subsequently, Modak *et al.* [21] reported theoretical TOECs for diamond determined by combining SOEC pressure derivatives, calculated using density functional theory, with results from shock wave propagation simulations using classical molecular dynamics employing an empirical interatomic potential. More recently, revised values [22] for the experimental TOECs, which corrected the errors in the previously reported SOEC pressure derivatives [20], were reported. With the availability of the revised experimental TOEC values, an assessment of the different theoretical approaches to accurately calculate the TOECs of diamond is in order.

Here we present a theoretical determination of the TOECs of diamond from density functional theory (DFT) calculations using the method of homogeneous deformations. Two different approaches were used to obtain the TOECS: (1) fitting TOECs to calculated energy-strain states, similar to Ref. [23], and (2) fitting TOECs to the calculated longitudinal stress-uniaxial strain states and to the calculated pressure derivatives of the SOECs. The second approach provides a more direct comparison with the experimental measurements [18–20,22]. The results of these calculations are compared with the experimental results and with previous theoretical determinations of the TOECs, providing a robust theoretical approach to the calculation of the nonlinear elastic response of strong solids.

II. THEORETICAL METHODS

The diamond elastic constants were calculated by using the method of homogeneous deformations [11,24] to combine continuum elasticity theory with total energy and stress calculations determined from first-principles methods. The continuum elasticity theory and first-principles computational methods used in this work are briefly summarized here, together with the energy-strain and longitudinal stress-uniaxial strain fitting approaches used to determine the TOECs.

A. Continuum elasticity theory

Let a_i be the initial coordinates of a material element in a body and let $x_i' = x_i(a_j)$ be the coordinates after application of a homogeneous elastic deformation. The deformation of the material system is described by the deformation gradient

$$F_{ij} = \frac{\partial x_i}{\partial a_j}. \tag{1}$$

The symmetric finite Lagrangian strain tensor (negative in compression) is then defined by

$$\eta_{ij} = \frac{1}{2}\sum_k (F_{ki}F_{kj} - \delta_{ij}). \tag{2}$$

Elastic constants are defined by expanding the internal energy per unit mass U as a Taylor series in strain at constant entropy [11,24,25]

$$\rho_0 U(\eta_{ij},S) = \rho_0 U(0,S) + \frac{1}{2}\sum_{ijkl} C^S_{ijkl}\eta_{ij}\eta_{kl} + \frac{1}{6}\sum_{ijklmn} C^S_{ijklmn}\eta_{ij}\eta_{kl}\eta_{mn} + \cdots, \tag{3}$$

where ρ_0 is the mass density of the material in the stress-free initial state. The expansion coefficients of the Taylor series in Eq. (3) are the isentropic elastic constants [11,24,25]

$$C^S_{ijkl} = \rho_0 \left.\frac{\partial^2 U}{\partial\eta_{ij}\partial\eta_{kl}}\right|_{\eta=0} \quad \text{(SOEC)}, \tag{4}$$

$$C^S_{ijklmn} = \rho_0 \left.\frac{\partial^3 U}{\partial\eta_{ij}\partial\eta_{kl}\partial\eta_{mn}}\right|_{\eta=0} \quad \text{(TOEC)}. \tag{5}$$

It is convenient to introduce stress-strain coefficients, defined as [11]

$$B_{ijkl} = \frac{\partial\sigma_{ij}}{\partial\eta_{ij}} = \frac{1}{2}(\sigma_{ik}\delta_{jl} + \sigma_{il}\delta_{jk} + \sigma_{jl}\delta_{ik} + \sigma_{jk}\delta_{il} - 2\sigma_{ij}\delta_{kl}) + C_{ijkl}, \tag{6}$$

where the σ_{ij} are applied Cauchy stresses in the current (strained) configuration. In the case of hydrostatic stress ($\sigma_{ij} = -P\delta_{ij}$) applied to a cubic crystal, Eq. (6) reduces to

$$B_{11} = C_{11} - P, \tag{7}$$

$$B_{12} = C_{12} + P, \tag{8}$$

$$B_{44} = C_{44} - P. \tag{9}$$

Here and in the remainder of this paper we use the contracted (Voigt) notation [11,24,25] (11 →1, 22 →2, 33 →3, 23 →4, 13 →5, 12 →6) for tensor indices to express C_{ijkl} and C_{ijklmn} as $C_{\alpha\beta}$ and $C_{\alpha\beta\gamma}$, respectively.

To calculate TOECs using the method of homogeneous deformations, the total energy of the strained diamond crystals was calculated using first-principles methods, and the TOECs were determined by fitting the calculated energy-strain results to Eq. (3) [23]. Alternatively, the stress state of the strained crystals was calculated and the results were fit to the derivative of Eq. (3) [17].

B. First-principles methods

In this work we used the Vienna *ab initio* simulation package (VASP) [26] density functional theory (DFT) code to carry out first-principles total energy and stress calculations using a plane-wave basis set at 0 K. Electron-ion interactions were described using projector-augmented wave pseudopotentials [27] within both the local density approximation (LDA) [28] and the PBE formulation of the generalized gradient approximation (GGA) [29]. High accuracy in evaluating the total energy is necessary to compute the TOECs, and convergence tests showed that a large energy cutoff ($E_{\text{cutoff}} =$ 1500 eV) was necessary to achieve convergence of the TOECs. A Γ-centered Monkhorst-Pack k-point grid of $13 \times 13 \times 13$ was used. Energies were calculated using the tetrahedron method with Blöchl corrections. The simulation cells used for cubic diamond in this work were composed of eight atoms, whose internal coordinates were relaxed for each applied deformation. The tolerances for the energy convergence of the self-consistent field loop and the maximum forces on the atoms in the ionic relaxation procedure were 10^{-8} eV and 10^{-4} eV/Å, respectively.

Homogeneous deformations were applied using the deformation gradient F_{ij}, obtained by inverting Eq. (2) to determine the crystal lattice vectors $\mathbf{r}_\mathbf{i}'$ of the deformed unit cell from the unstrained lattice vectors $\mathbf{r}_\mathbf{i}$:

$$\mathbf{r}_i' = F_{ij}\mathbf{r}_j. \tag{10}$$

For each applied deformation, a conjugate-gradient relaxation of the crystal internal coordinates was performed for the deformed cell, minimizing the total energy of the strained crystal.

C. Energy-strain approach

In this approach the calculation of TOECs is based on Eq. (3), as described previously by Zhao *et al.* [23]. For a cubic crystal, calculations incorporating six different strain tensors are required to determine the six TOECs. The strain tensors η_{ij} used in this work are listed in the Appendix as (A1)–(A6). The nonzero components of each strain tensor were written in terms of a single parameter ξ, conveniently reducing Eq. (3) to an expansion in terms of a single variable:

$$\rho_0[U(\xi) - U(0)] = \tfrac{1}{2}K_2\xi^2 + \tfrac{1}{6}K_3\xi^3 + O(\xi^4), \tag{11}$$

where $U(0)$ is the energy of the unstrained state. Using Eq. (11), the calculated total energies were fit to a fourth-order polynomial to determine K_2 and K_3 for each strain. K_2 and K_3,

for strains (A1)–(A6), provide a system of equations (Table IV in the Appendix) that were solved for the SOECs and TOECs.

As shown in previous calculations for silicon [23], the fitted values of K_2 and K_3 in Eq. (11) are insensitive to the choice of maximum strains used in the fit over a certain range. Here we use $-0.08 \leqslant \xi \leqslant 0.06$ with a strain step size of $\Delta\xi = 0.004$. Changing $\Delta\xi$ to a smaller value had a negligible effect on the elastic constants.

D. Longitudinal stress-uniaxial strain approach

To facilitate a more direct comparison to what is measured in the shock wave experiments [18,19], longitudinal stresses were calculated for three uniaxial strain tensors, corresponding to the different shock wave compression directions examined in the experiments: [100], [110], and [111]. The longitudinal elastic constants C'_{11} and C'_{111} are defined here by an expansion of the longitudinal stress to second order in uniaxial strain η'_1:

$$\sigma'_1 = \frac{\rho_0}{\rho}\left(C'_{11}\eta'_1 + \frac{1}{2}C'_{111}\eta'^2_1\right), \tag{12}$$

where the primed tensor variables are expressed in a coordinate system that is aligned with the direction of shock compression. Equation (12) is identical to the equation used previously [18] to analyze the experimental shock wave compression results. The strain step size for the longitudinal stress calculations was $\Delta\xi = 0.004$ and the maximum strain was $\xi = -0.08$. The uniaxial Lagrangian strains were determined in terms of the density compression ratio for the compressed (ρ) and uncompressed (ρ_0) crystal:

$$\eta'_1 = \frac{1}{2}\left(\frac{\rho_0^2}{\rho^2} - 1\right). \tag{13}$$

The calculated longitudinal stress-uniaxial strain results were fit using Eq. (12) to provide three equations containing linear combinations of the TOECs [see (A7)–(A9) in the Appendix]. To determine the complete set of six TOECs, the pressure derivatives of the SOECs were calculated to provide three additional equations [see (A10)–(A12) in the Appendix]. These six equations were solved to determine the six TOECs for diamond.

The SOEC pressure derivatives were calculated by relaxing the diamond unit cell to −10, 0, and 10 GPa external hydrostatic stress and then applying small secondary deformations. For each hydrostatic stress state, the stress-strain coefficients $B_{\alpha\beta}$, defined in Eq. (6), were determined using a linear fit to the calculated stresses for the deformed diamond lattice. The pressure derivatives of the $C_{\alpha\beta}$ were calculated by differentiating Eqs. (7)–(9).

III. DETERMINATION OF THIRD-ORDER ELASTIC CONSTANTS

A. Energy-strain approach

We present our results for the unstrained lattice constants, ambient densities, and elastic constants up to third order calculated using the energy-strain approach [23] for both LDA and PBE in Table I alongside previous theoretical and experimental determinations of the same [14–17,20–22]. The lattice constants and densities for LDA and PBE in this work match the experimental values well. The error between calculated and experimental values for LDA (PBE) in the lattice constant is 1% (0.1%) and in density is 3% (0.3%). As shown in Table I, the LDA lattice constant is somewhat smaller than that obtained using PBE. Consistent with the smaller lattice constants, the LDA SOECs are larger than the PBE SOECs, reflecting a larger stiffness, and the LDA TOECs are either larger or of a similar magnitude compared to the PBE TOECs. Differences between the LDA and PBE results are relatively small for the TOECs (2%–5%) and larger for the SOECs (5%–20%). In calculating the TOEC C_{456}, compressive strains larger than $\xi = -0.048$ for the (A6) strain yielded a different relaxed structure than the lower magnitude strains, which caused the energy-strain relationship to diverge. Therefore, the fitted value of C_{456} reported in Table I was evaluated using $-0.048 \leqslant \xi \leqslant 0.06$.

TABLE I. Lattice constant (Å), density (g/cm^3), and the second- and third-order elastic constants of diamond (GPa). The elastic constants presented here were calculated using the energy-strain approach. Previous theoretical results [14–17,21] and experimental results [20,22] are also shown for comparison.

	Previous theory						Present theory	
	Ref. [14]	Ref. [15]	Ref. [16]	Ref. [17]	Ref. [21]	Experiment	LDA	PBE
a	–	–	–	3.55	–	3.567	3.533	3.570
ρ_0	–	–	–	3.567	–	3.517	3.619	3.508
C_{11}	–	–	–	1050 ± 10	1065	1079 ± 5[a]	1104	1054
C_{12}	–	–	–	127 ± 4	122	124 ± 5[a]	148	124
C_{44}	–	–	–	550 ± 5	568	578 ± 2[a]	593	559
C_{111}	−6260	−7367	−6475	−6300 ± 300	−7290	−7600 ± 600[b]	−6303	−6026
C_{112}	−2260	−2136	−1947	−800 ± 100	−1398	−1270 ± 570[b]	−1739	−1643
C_{123}	112	1040	982	0 ± 400	−247	−330 ± 920[b]	589	606
C_{144}	−674	186	115	0 ± 300	−592	2390 ± 850[b]	−196	−200
C_{166}	−2860	−3292	−2998	−2600 ± 100	−2863	−4100 ± 380[b]	−2911	−2817
C_{456}	−823	76	−135	−1300 ± 100	−2991	−2890 ± 750[b]	−1074	−1168

[a]Reference [20].
[b]Reference [22].

TABLE II. Experimental and calculated longitudinal second-order elastic constants (C'_{11}), longitudinal third-order elastic constants (C'_{111}), and pressure derivatives of the second-order elastic constants.

		Present theory	
	Experiment[a]	LDA	PBE
$C'^{[100]}_{11}$	1079 ± 5	1083 ± 4	1033 ± 5
$C'^{[110]}_{11}$	1180 ± 7	1163 ± 13	1094 ± 12
$C'^{[111]}_{11}$	1213 ± 8	1214 ± 10	1139 ± 9
$C'^{[100]}_{111}$	−7603 ± 600	−7828 ± 154	−7515 ± 143
$C'^{[110]}_{111}$	−15146 ± 1067	−15741 ± 400	−15183 ± 383
$C'^{[111]}_{111}$	−14631 ± 1183	−14949 ± 314	−14385 ± 289
dC_{11}/dP	6.98 ± 0.7	6.09	6.26
dC_{12}/dP	2.06 ± 0.7	1.94	1.94
dC_{44}/dP	3.98 ± 0.3	3.83	3.99

[a]References [18,22].

Comparing the TOECs calculated here with the measured TOECs [22], we find that C_{111}, C_{144}, C_{166}, and C_{456} show significant differences (as large as 110%) with experimentally determined values. Only C_{112} and C_{123} lie within the error bounds of the experimental results. The TOECs calculated previously using a first-principles approach in Ref. [17] are consistent with the present results and show similar disagreement with the experimental results. Although the TOECs calculated previously [14–16] differ significantly among themselves, our calculated TOECs lie within the scatter of the previous theoretical results.

With the exception of C_{144} and C_{166}, the TOECs calculated by Modak *et al.* [21] provide a somewhat better overall match to the measured TOECs, compared to the other calculated results. However, their approach relies upon a combination of *ab initio* calculations and classical molecular dynamics simulations using empirical potentials. Hence the TOECs reported in [21] were not all calculated at the same level of theory.

To gain insight into the differences between the theoretically calculated TOECs (obtained with the energy-strain method) and the experimental results, we now turn to a more direct comparison between theory and experiment, using the methods of Sec. II D.

B. Longitudinal stress-uniaxial strain approach

The second- and third-order longitudinal elastic constants (C'_{11} and C'_{111}, respectively) for uniaxial compressions along [100], [110], and [111] were determined by fitting the calculated longitudinal stress to Eq. (12). Table II shows that the C'_{11} calculated using PBE are smaller than the LDA results by 4%–9% but differences in the C'_{111} are smaller between the two functionals (less than 4%). C'_{11} and C'_{111} calculated using LDA agree well with experiment for all orientations, as do the PBE values for C'_{111}. The error bars for the DFT results are statistical uncertainties from the covariance matrix of the fit to Eq. (12).

Calculated longitudinal stress-uniaxial strain results are shown in Fig. 1 for compressions along (a) [100], (b) [110], and (c) [111] directions. The calculated longitudinal stress-strain curves (red and blue for LDA and PBE, respectively) show good agreement with the experimental results (black squares and black curves), especially for LDA, where the theoretical and experimental curves nearly overlap each other.

To determine the TOECs, the calculated longitudinal stress-uniaxial strain results were augmented with the calculated SOEC pressure derivatives, as discussed in Sec. II D. As shown in Table II, the calculated pressure derivatives dC_{12}/dP and dC_{44}/dP are in good agreement with the measured results and the calculated value for dC_{11}/dP lies just outside the experimental uncertainty bounds [20,22].

The TOECs were determined by solving Eqs. (A9)–(A14) and are shown in Table III, together with the measured TOECs. The calculated TOECs show good agreement with the experimental results and all are within the experimental error bounds. The difference between the calculated and measured [22] pressure derivative dC_{11}/dP is the largest source of the disagreement between the calculated and measured TOECs, primarily affecting C_{112} and C_{123} [see Eqs. (A9)–(A14)]. Calculations using the LDA and PBE functionals show similar results, with the LDA TOECs being somewhat larger in magnitude those calculated using PBE. For all TOECs, the

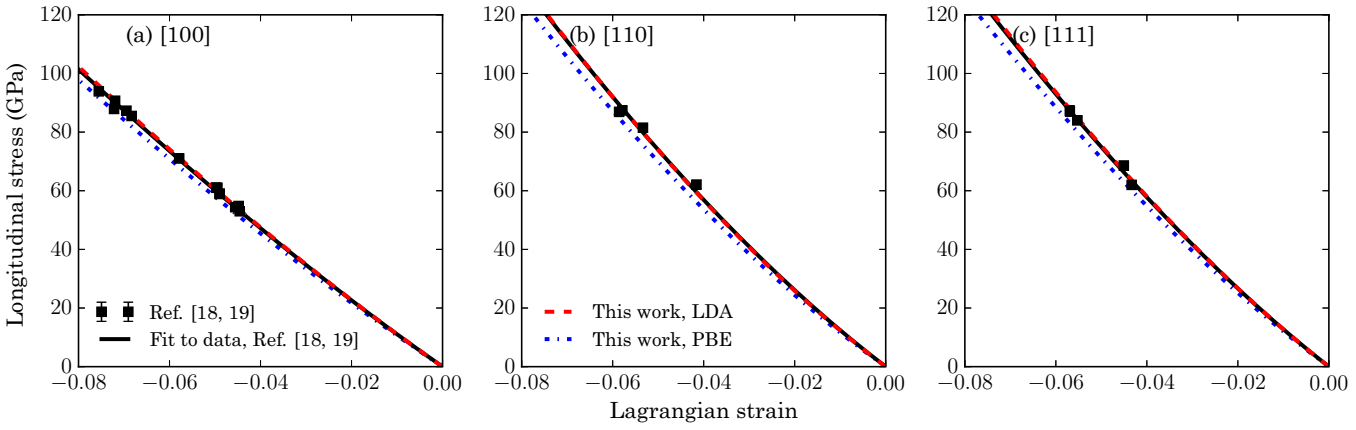

FIG. 1. Longitudinal stress versus uniaxial strain for diamond shock compressed along (a) [100], (b) [110], and (c) [111] directions. The black squares are measured states from Refs. [18,19]. The solid black curve is a fit to the measured states, the red dashed and blue dot-dashed curves are DFT calculations using the LDA and PBE functionals, respectively.

TABLE III. Third-order elastic constants of diamond determined from calculated longitudinal stress-uniaxial strain results and the pressure derivatives of the second-order elastic constants.

		Present theory	
	Experiment [22]	LDA	PBE
C_{111}	-7600 ± 600	-7828 ± 154	-7515 ± 143
C_{112}	-1270 ± 570	-901 ± 92	-845 ± 86
C_{123}	-330 ± 920	-1062 ± 188	-960 ± 176
C_{144}	2390 ± 850	2783 ± 283	2693 ± 271
C_{166}	-4100 ± 380	-4369 ± 134	-4223 ± 128
C_{456}	-2890 ± 750	-2983 ± 189	-2870 ± 175

statistical errors shown in Table III were much smaller than the experimental uncertainties.

We note that our theoretical results calculated at $T = 0$ K provide good agreement with the experimental results [18,22], despite the temperature increase inherent in the previous shock wave compression. This is because the extreme stiffness of diamond causes modest elastic compressions in the shock experiments and, as a result, the corresponding temperature increases in the shocked diamond were extremely small. To examine the nonlinear elastic response of strong single crystals at higher temperatures, the SOECs and TOECs must be incorporated into an anisotropic thermoelastic framework (see, for example, Ref. [24]). However, such developments are not considered here.

C. Discussion

Comparing the results presented in Secs. III A and III B, it is seen that the TOECs calculated using the longitudinal stress-uniaxial strain approach show significantly better agreement with the experimental results [18,19,22], compared to those calculated using the energy-strain approach. Because the same first-principles methods were used for the energy-strain approach and the longitudinal stress-uniaxial strain approach, the differences in the TOECs calculated using the two approaches is likely due to differences in the analysis and fitting of the calculated energies and stresses. These differences are discussed next.

Examination of Eqs. (A7)–(A12), which are similar to those used to analyze and fit the data from the diamond shock compression experiments [18,19], shows that some TOECs appear more frequently, or with larger coefficients, than others in the system of linear equations. As a result, some of the TOECs are not as well constrained by the experiments as others. In particular, C_{166} appears more often and is weighted more heavily in Eqs. (A7)–(A12) than C_{123}, C_{144}, and C_{456}. Therefore, C_{166} is more well constrained than C_{123}, C_{144}, and C_{456}, and accordingly has a smaller experimental uncertainty. Because the TOECs calculated using the longitudinal stress-uniaxial strain approach were determined using similar equations (A7)–(A12) as those used to analyze the experimental results [18,19], the TOECs calculated using this approach were determined under the same constraints as those determined from the experimental results. Because the TOECs calculated using the energy-strain approach were determined using a different set of equations (see Table IV), the calculated TOECs were constrained differently. As as result, the TOECs calculated using the energy-strain approach did not match the experimental results as well as those determined using the longitudinal stress-uniaxial strain approach.

TABLE IV. The coefficients K_2 and K_3 used in the energy expansion of Eq. (11), expressed as combinations of SOECs and TOECs for a cubic crystal, using (A1)–(A6) [23].

Strain	K_2	K_3
(A.1)	C_{11}	C_{111}
(A.2)	$2C_{11} + 2C_{12}$	$2C_{111} + 6C_{112}$
(A.3)	$3C_{11} + 6C_{12}$	$3C_{111} + 18C_{112} + 6C_{123}$
(A.4)	$C_{11} + 4C_{44}$	$C_{111} + 12C_{144}$
(A.5)	$C_{11} + 4C_{44}$	$C_{111} + 12C_{166}$
(A.6)	$12C_{44}$	$48C_{456}$

In the determination of TOECs from the experimental shock compression data [18,19,22], the measured longitudinal stresses were fit to a quadratic function of strain [Eq. (12)] because fitting to a higher order expansion was unwarranted, given the limited data set available. Therefore, the extent to which the measured TOECs were affected by the higher-order elastic response (fourth-order elastic constants, etc.) of the material could not be determined. The same issue also arises for the TOECs calculated using the longitudinal stress-uniaxial strain approach because the calculated results were analyzed using Eq. (12). In contrast, the calculated energy-strain results were analyzed using Eq. (11), which incorporates terms containing fourth-order elastic constants to mitigate the effect of the higher-order elastic response. Thus, the two methods differ regarding the truncation of the Taylor series in Eq. (3). Examining the calculated and measured values for C_{111}, we note that C_{111} calculated using the longitudinal stress-uniaxial strain approach (Table III) matches the measured value well [18,19], but differs significantly from that calculated using the energy-strain approach (Table I). Therefore, because C_{111} was calculated using the same strain (A1) for both theoretical approaches, our results suggest that the higher order elastic response (fourth-order elastic constants, etc.) plays a role in the differences observed in the TOECs calculated using the two different theoretical approaches.

Overall, our results show that the details of the TOEC analysis and fitting procedures play an important role when making comparisons between different theoretical and experimental approaches for determining the TOECs. The work presented here shows that evaluation of the different theoretical approaches for calculating the TOECs is best carried out using calculations and analysis procedures that are closely aligned to the experimental approach.

IV. CONCLUSIONS

To demonstrate the use of first-principles methods for determining the nonlinear elastic response of strong solids, density functional theory was used to calculate the third-order elastic constants (TOECs) of diamond. Two different approaches were used: an energy-strain approach and a longitudinal stress-uniaxial strain approach. The TOECs calculated

using the longitudinal stress-uniaxial strain approach provided a good overall match to the experimentally determined TOECs [22]. Also, the longitudinal stress-uniaxial strain calculations provided a good match to the physical variables that were measured directly in previous shock compression experiments [18,19]. The present results demonstrate that first-principles approaches can be used to accurately calculate the TOECs of diamond.

Although the TOECs calculated using the energy-strain approach were within the scatter of the values determined in previous theoretical studies [14–17,21], they differed significantly from the experimentally determined TOECs [22] and the TOECs calculated using the longitudinal stress-uniaxial strain approach. The differences between the TOECs calculated using the two approaches can be understood in terms of differences in the analysis and fitting of the calculated energies and stresses. In particular, the series in Eq. (3) was truncated differently in the two different approaches. The significantly better match to the measured TOECs provided by the longitudinal stress-uniaxial strain approach, compared to the energy-strain approach presented here and in previous theoretical studies [14–17], is due to the close alignment of the analysis procedures used in the longitudinal stress-uniaxial strain approach with the procedures used in the experimental determination [18,19,22].

Although the work presented here has focused on diamond, the theoretical methods used to determine the TOECs are general. Therefore, the theoretical methods presented here are also expected to provide an accurate description of the nonlinear elastic response of other strong solids.

ACKNOWLEDGMENTS

This work was supported by the Department of Energy/NNSA through the Cooperative Agreement No. DE-NA0002007 with Washington State University.

APPENDIX: STRAIN TENSORS AND ANALYTICAL RELATIONS FOR THE DETERMINATION OF TOECs

In (A1)–(A6) we list the Lagrangian strain tensors η_{ij} used in the energy-strain calculations presented here:

$$\eta_{ij} = \begin{bmatrix} \xi & 0 & 0 \\ 0 & 0 & 0 \\ 0 & 0 & 0 \end{bmatrix}, \tag{A1}$$

$$\eta_{ij} = \begin{bmatrix} \xi & 0 & 0 \\ 0 & \xi & 0 \\ 0 & 0 & 0 \end{bmatrix}, \tag{A2}$$

$$\eta_{ij} = \begin{bmatrix} \xi & 0 & 0 \\ 0 & \xi & 0 \\ 0 & 0 & \xi \end{bmatrix}, \tag{A3}$$

$$\eta_{ij} = \begin{bmatrix} \xi & 0 & 0 \\ 0 & 0 & \xi \\ 0 & \xi & 0 \end{bmatrix}, \tag{A4}$$

$$\eta_{ij} = \begin{bmatrix} \xi & \xi & 0 \\ \xi & 0 & 0 \\ 0 & 0 & 0 \end{bmatrix}, \tag{A5}$$

$$\eta_{ij} = \begin{bmatrix} 0 & \xi & \xi \\ \xi & 0 & \xi \\ \xi & \xi & 0 \end{bmatrix}. \tag{A6}$$

For each of the strains (A1)–(A6), the coefficients K_2 and K_3 used in the energy-strain fitting function [Eq. (11)] are expressed in terms of the SOECs and TOECs in Table IV. When incorporated into Eq. (11), the results in Table IV provide six equations to solve for the six TOECs of diamond.

For the longitudinal stress-uniaxial strain approach, the system of six equations used to solve for the TOECs is

$$C'^{[100]}_{111} = C_{111}, \tag{A7}$$

$$C'^{[110]}_{111} = \frac{1}{4}(C_{111} + 3C_{112} + 12C_{166}), \tag{A8}$$

$$C'^{[111]}_{111} = \frac{1}{9}(C_{111} + 6C_{112} + 2C_{123} + 12C_{144} + 24C_{166} + 16C_{456}), \tag{A9}$$

$$C^M_{111} + 2C^M_{112} = -\frac{dC_{11}}{dP}(C_{11} + 2C_{12}) - C_{11}, \tag{A10}$$

$$C^M_{112} + 2C^M_{123} = -\frac{dC_{12}}{dP}(C_{11} + 2C_{12}) - C_{12}, \tag{A11}$$

$$C^M_{144} + 2C^M_{166} = -\frac{dC_{44}}{dP}(C_{11} + 2C_{12}) - C_{44}, \tag{A12}$$

where C^M_{ijk} are the mixed third-order isentropic-isothermal elastic constants [11]. Because the thermal expansion coefficient of diamond is very small, differences between the mixed elastic constants and the isentropic elastic constants are negligible.

[1] J. E. Lowther, The role played by computation in understanding hard materials, Materials **4**, 1104 (2011).
[2] J. Narayan and A. Bhaumik, Research update: Direct conversion of amorphous carbon into diamond at ambient pressures and temperatures in air, APL Mater. **3**, 100702 (2015).
[3] A. Friedrich, B. Winkler, L. Bayarjargal, W. Morgenroth, E. A. Juarez-Arellano, V. Milman, K. Refson, M. Kunz, and K. Chen, Novel Rhenium Nitrides, Phys. Rev. Lett. **105**, 085504 (2010).
[4] Y. Palyanov, A. Sokol, A. Khokhryakov, and A. Kruk, Conditions of diamond crystallization in kimberlite melt: Experimental data, Russian Geol. Geophys. **56**, 196 (2015).
[5] P. Niedermann, W. Hänni, N. Blanc, R. Christoph, and J. Burger, Chemical vapor deposition diamond for tips in nanoprobe experiments, J. Vacuum Sci. Technol. A **14**, 1233 (1996).
[6] W. B. Holzapfel, Physics of solids under strong compression, Rep. Prog. Phys. **59**, 29 (1996).
[7] V. P. Grichko and O. A. Shenderova, in *Ultrananocrystalline Diamond*, edited by O. A. Shenderova and D. M. Gruen (William Andrew, Norwich, NY, 2006), pp. 529–557.
[8] X. Zhao, M. C. Nguyen, C. Z. Wang, and K. M. Ho, New stable Re–B phases for ultra-hard materials, J. Phys. Condens. Matter **26**, 455401 (2014).

[9] J. J. Swab, L. Vargas-Gonzalez, E. Wilson, and E. Warner, Properties and performance of polycrystalline cubic boron nitride, Int. J. Appl. Ceram. Tec. **12**, E74 (2015).
[10] D. Wallace, *Thermodynamics of Crystals* (Dover, New York, 1998).
[11] D. C. Wallace, *Solid State Physics* (Academic, New York, 1970), Vol. 25, p. 301.
[12] Y. Hiki, Higher order elastic constants of solids, Annu. Rev. Mater. Sci. **11**, 51 (1981).
[13] D. G. Clerc and H. Ledbetter, Second-order and third-order elastic properties of diamond: An *ab initio* study, J. Phys. Chem. Solids **66**, 1589 (2005).
[14] M. H. Grimsditch, E. Anastassakis, and M. Cardona, Effect of uniaxial stress on the zone-center optical phonon of diamond, Phys. Rev. B **18**, 901 (1978).
[15] E. Anastassakis, A. Cantarero, and M. Cardona, Piezo-Raman measurements and anharmonic parameters in silicon and diamond, Phys. Rev. B **41**, 7529 (1990).
[16] C. S. G. Cousins, Elasticity of carbon allotropes. I. Optimization, and subsequent modification, of an anharmonic Keating model for cubic diamond, Phys. Rev. B **67**, 024107 (2003).
[17] O. H. Nielsen, Optical phonons and elasticity of diamond at megabar stresses, Phys. Rev. B **34**, 5808 (1986).
[18] J. M. Lang and Y. M. Gupta, Experimental Determination of Third-Order Elastic Constants of Diamond, Phys. Rev. Lett. **106**, 125502 (2011).
[19] J. M. Lang, Mechanical and optical response of diamond crystals shock compressed along different orientations, Ph.D. thesis, Washington State University, 2013.
[20] H. J. McSkimin and P. Andreatch, Elastic moduli of diamond as a function of pressure and temperature, J. Appl. Phys. **43**, 2944 (1972).
[21] P. Modak, A. K. Verma, and S. M. Sharma, Determination of the third-order elastic constants of diamond by shock wave simulations, Europhys. Lett. **110**, 56003 (2015).
[22] J. Winey, A. Hmiel, and Y. Gupta, Third-order elastic constants of diamond determined from experimental data, J. Phys. Chem. Solids **93**, 118 (2016).
[23] J. Zhao, J. M. Winey, and Y. M. Gupta, First-principles calculations of second- and third-order elastic constants for single crystals of arbitrary symmetry, Phys. Rev. B **75**, 094105 (2007).
[24] R. N. Thurston, Physical acoustics: Principles and methods, in *Physical Acoustics*, edited by W. P. Mason and R. N. Thurston (Academic, New York, 1964).
[25] K. Brugger, Thermodynamic definition of higher order elastic coefficients, Phys. Rev. **133**, A1611 (1964).
[26] G. Kresse and J. Furthmüller, Efficient iterative schemes for *ab initio* total-energy calculations using a plane-wave basis set, Phys. Rev. B **54**, 11169 (1996).
[27] P. E. Blöchl, Projector augmented-wave method, Phys. Rev. B **50**, 17953 (1994).
[28] D. M. Ceperley and B. J. Alder, Ground State of the Electron Gas by a Stochastic Method, Phys. Rev. Lett. **45**, 566 (1980).
[29] J. P. Perdew, K. Burke, and M. Ernzerhof, Generalized Gradient Approximation Made Simple, Phys. Rev. Lett. **77**, 3865 (1996).